Biosensors and Bioelectronics 100 (2018) 274–281

Contents lists available at ScienceDirect

Biosensors and Bioelectronics

journal homepage: www.elsevier.com/locate/bios

Tetrahedral DNA probe coupling with hybridization chain reaction for competitive thrombin aptasensor

Ying-Xu Chen[a,b], Ke-Jing Huang[a,b,*], Liu-Liu He[a,b], Yi-Han Wang[a,b]

[a] College of Chemistry and Chemical Engineering, Xinyang Normal University, Xinyang 464000, China
[b] Institute for Conservation and Utilization of Agro-bioresources in Dabie Mountains, Xinyang Normal University, Xinyang 464000, China

ARTICLE INFO

Keywords:
Sulfur and nitrogen co-doped reduced graphene oxide
Tetrahedral DNA
Thrombin
Hybridization chain reaction
Aptasensor

ABSTRACT

A novel competitive aptasensor for thrombin detection is developed by using a tetrahedral DNA (T-DNA) probe and hybridization chain reaction (HCR) signal amplification. Sulfur and nitrogen co-doped reduced graphene oxide (SN-rGO) is firstly prepared by a simple reflux method and used for supporting substrate of biosensor. Then, T-DNA probe is modified on the electrode by Au-S bond and a competition is happened between target thrombin and the complementary DNA (cDNA) of aptamer. The aptamer binding to thrombin forms an aptamer-target conjugate and make the cDNA remained, and subsequently hybridizes with the vertical domain of T-DNA. Finally, the cDNAs trigger HCR, which results in a great current response by the catalysis of horseradish peroxidase to the hydrogen peroxide + hydroquinone system. For thrombin detection, the proposed biosensor shows a wide linearity range of 10^{-13}–10^{-8} M and a low detection limit of 11.6 fM (S/N = 3), which is hopeful to apply in biotechnology and clinical diagnosis.

1. Introduction

Protein is a crucial ingredient which makes up whole cell and tissue of human (Li et al., 2017). The vital parts of body all need proteins' participation, so the detection of protein fleetly and accurately in disease diagnosis is particularly important with the increasing importance of precision medicine (Lv et al., 2017; Cardoso et al., 2017). Thrombin, a serine protease produced from inactive zymogen prothrombin through a sequence of enzyme fission processes in humans (Du et al., 2016), is the dominating proteinase in the blood coagulation system, possessing many procedures in phlogosis and tissue repair at the vascular wall (Ye et al., 2017). The concentration of thrombin in blood is different in various conditions. It is not present in blood under normal conditions. However, it can reach low-micromolar concentrations during the coagulation process, and low levels (low nM) of thrombin generated early in hemostasis are also important to the overall process (Shuman and Majerus, 1976). Out of the hemostatic process, circulating thrombin has been detected at high-picomolar range in blood of patients suffering from diseases known to be associated with coagulation abnormalities (Bichler et al., 1996). Hence, it would be remarkably ponderable to fabricate a rapid and sensitive pathway for detecting thrombin.

The traditional methods of monitoring thrombin are enzyme-linked immunosorbent assay (Pelzer et al., 1988), radioimmunoassay (Shuman et al., 1976) and so on. However, antibodies used in these methods are expensive, hard to operate, need more time and manpower, and the preparation and preservation of antibodies are difficult. The aptamer-based sensing platform draws increasing attention of researchers in recent years (Nguyen et al., 2017; Jeddi et al., 2017). Aptamer is a single-stranded oligonucleotide, which is entirely designed from random-sequence DNA or RNA libraries in an extracorporeal choice procedure that can bundle many types of target molecules with affinity and specificity (Ellington et al., 1990; Hou et al., 2017), such as small inorganic (Tan et al., 2017), organic substances (Li et al., 2016), protein (Yang et al., 2017) and cell (Chen et al., 2016a). Most of all, aptamer-based sensing strategies exert visible merits compared with traditional methods, including low cost, simple synthesis, good chemical stability and close binding force, which make aptamers are extensively applied in the fabrication of multifarious biosensor (Ha et al., 2017; Taghdisi et al., 2016). For human thrombin, there is an aptamer with 29 bases DNA oligonucleotide which can bind to the heparin-binding exosite of thrombin (Zhao et al., 2015). In this circumstance, it's appropriate to fabricate detecting methods for thrombin that utilizes the firm binding force of the thrombin and its corresponding aptamer. Electrochemical method is an acknowledged and befitting technique for fast, sensitive and selective detection of thrombin (Zhao et al., 2017). The primary difficulty is the grasp of density and orientation of molecules at the electrode surface. In order to solve this problem, a tetrahedral DNA

* Corresponding author at: College of Chemistry and Chemical Engineering, Xinyang Normal University, Xinyang 464000, China.
E-mail address: kejinghuang@163.com (K.-J. Huang).

http://dx.doi.org/10.1016/j.bios.2017.09.022
Received 11 July 2017; Received in revised form 9 September 2017; Accepted 14 September 2017
Available online 15 September 2017
0956-5663/

nanostructure (T-DNA) based holder has been developed, which is consist of 4 single-stranded DNAs (Lin et al., 2016). This kind of stereo structure can exactly control the assembled probe DNA on the electrode interface and rise above the spatial effect of a conventional single-stranded probe to increase accessibility and reactivity, and prevent the entrance of spacer molecules (Poturnayová et al., 2015; Huang et al., 2015; Miao et al., 2015).

For the sake of obtaining a low detection limit for the thrombin sensor, a variety of signal amplification techniques are induced. Hybridization chain reaction (HCR) is an isothermal method for signal amplification without the participation of any bio-enzymes or thermal cycler (Dirks et al., 2004; Liu et al., 2016). Hence, many limitations of relevant enzymatic methods like pinpoint control of pH, temperature and buffer media can be avoided, leading to a widespread application of HCR for constructing the sensing platform. In addition, r using nanomaterials for signal amplification is another suitable element because they commonly possess big specific area to immobilize more signal molecules at the electrode interface, and is favorable to speed up the electron transfer (Wang et al., 2017; Singh et al., 2016). Graphene oxide (GO), its particular electronical, physical, and chemical performances have made it a hopeful option for various application in biosensor (Huang et al., 2016, 2014). Substitutive adulteration with ethnic sulfur and nitrogen atoms into the carbon net can adjust the chemical performances, produce new vivid sites, and markedly facilitate the catalytic activity of GO (Duan et al., 2015). Additionally, co-doping by two elements with different electronegativities can induce a distinctive electron allocation and then issue in a synergistic effect (Chen et al., 2016b).

Au nanoparticles (AuNPs) are mostly recommended owing to the fact that they can greatly increase the current response of the modified sensor with a good conductive ability and immobilization of biomolecular by Au–S bond (Shuai et al., 2016), and have been widely used to construct aptamer sensors (Shuai et al., 2017; Kuang et al., 2016). The aforementioned standpoints have motivated the present assay. In this work, we prepare S, N co-doped reduced graphene oxide (SN-rGO) as electrode supporting substrate by an effective and simple reflux method. Then, gold nanoparticles (AuNPs) are electrodeposited and T-DNA probe is modified on the electrode by Au–S bond. A competitive aptasensor for the sensitive detecting thrombin is constructed by combining SN-rGO, T-DNA probe and HCR signal amplification. Besides, a complementary DNA (cDNA) is introduced which is competed with target thrombin of aptamers. By using the developed assay, thrombin can be detected with a low detection limit of 11.6 fM, which is significantly lower than other aptasensor. The results can be attributed to the good conductivity of SN-rGO, stable structure of T-DNA probe and HCR signal amplification strategy.

2. Experimental

2.1. Experimental reagent and instrument

Graphite powder, $(NH_4)_2S_2O_8$, $KMnO_4$, thiocarbamide, glycol, carbamide and Na_2S were purchased from Sigma Aldrich (St. Louis, MO). Thrombin, carcinoembryonic antigen (CEA), bovine serum albumin (BSA), platelet derived growth factor-BB (PDGF-BB) and hydroquinone (HQ) were obtained from Shanghai Xueman Biotechnology Co. Ltd (China). The DNA sequences were acquired from Shanghai Sangon Biological Engineering Technology Co. Ltd (Shanghai, China). All DNA sequences were synthesized by using standard phosphoramidite chemistry and purified using reversed phase HPLC. The sequences of synthetic DNA are shown in Table 1.

Cyclic Voltammetry (CV) and differential pulse voltammetry (DPV) were measured on an EC550 electrochemical workstation (Wuhan, Gaoss Union, China) and electrochemical impedance spectroscopy (EIS) working curves were recorded on a RST5200F electrochemical workstation (Zhengzhou Shi Rui Si Instrument, China). A conventional three-electrode system was used which made up of a glassy carbon electrode (GCE) working electrode, an Hg/Hg_2Cl_2 reference electrode and a platinum wire auxiliary electrode. The as-prepared materials were characterized by a Hitachi S-4800 scanning electron microscope (SEM, Tokyo, Japan), a JEM 2100 transmission electron microscope (TEM, JEOL, Tokyo, Japan) and a K-ALPHA 0.5EV X-ray Photoelectron Spectrometer (XPS, Thermo Fisher Scientific, UK.). Moreover, energy dispersive spectrum (EDS) analysis was attached to SEM for exploring elementary component.

2.2. Preparation of S, N co-doped reduced graphene oxide

GO was prepared by modified Hummer's method (Hummers et al., 1958). The SN-rGO was prepared according to reference (Bag et al., 2015). GO was first dispersed in 1 mg mL^{-1} glycol solution. 3 mM thiocarbamide's glycol solution was then added into the dispersion serving as dopant of S and N. Subsequently, the mixture was transferred to a round-bottom flask and kept at 180 °C for 3 h. After cooling to room temperature, the mixture was centrifuged and washed with DI water and ethanol, and then dried in vacuum drying oven at 60 °C for 10 h. The S-rGO and N-rGO were prepared with the similar process except that by using carbamide and Na_2S as dopants.

2.3. Preparation of tetrahedral DNA probe

The GCE was polished with 0.3 and 0.05 aluminium oxide slurry to obtain a mirror surface, followed by swashing with ethanol and ultrapure water to remove remaining impurities, and then dried by nitrogen. An 8 μL SN-rGO suspension (1 mg mL^{-1}) was dropped on GCE and dried in air to form a homogeneous membrane. After that, AuNPs were immobilized on the GCE by electrodeposition method in 0.1% $HAuCl_4$ with 0.1 M KNO_3 to obtain AuNPs/SN-rGO/GCE. The modification of tetrahedral DNA probe (T-DNA) on AuNPs/SN-rGO/GCE was carried out as follows: four ssDNAs (Tetrahedron A, B, C, D) were respective dissolved in 10 mM Tris-HCl buffer solution (10 mM TCEP, 50 mM $MgCl_2$, pH 8.0) to form a concentration of 4 μM. The four ssDNAs were mixed and heated at 95 °C for 2 min with the final concentration of 1 μM. After the mixture cooled to 4 °C in ice bath, T-DNA was formed and then 8 μL solution was applied on AuNPs/SN-rGO/GCE and incubated at 4 °C over night. The obtained T-DNA/AuNPs/SN- rGO/GCE was dipped in 4 μL MCH (0.5 mM) to eliminate the non-specificity adsorption of electrode surface and rinsed carefully before use.

2.4. Preparation of competitive aptasensor

2 μL aptamer (0.5 μM) was mixed with 5 μL thrombin and then incubated at 30 °C for 120 min. Subsequently, 2 μL cDNA (0.5 μM) was added and kept at 30 °C for 60 min. After that, the mixture was dropped on the T-DNA/AuNPs/SN-rGO/GCE and incubated at 30 °C for another 60 min. After thoroughly swashing, the electrode was treated with the mixture of H1 and H2 at room temperature for different time. Soon afterwards, 8 μL avidin-HRP (10 μg mL^{-1}) was covered on the electrode and incubated for 30 min at room temperature. In the end, the obtained biosensor was washed entirely with 10 mM PBS (pH 7.0).

2.5. Electrochemical measurement

Cyclic voltammetry (CV) was tested in 1.0 mM $[Fe(CN)_6]^{3/4-}$ solution including 0.1 M KCl with a potential range from − 0.2V to 0.6 V and the scan rate of 100 mV s^{-1}. The electrodeposition experiment was carried out in 0.1% $HAuCl_4$ solution containing 0.1 M KNO_3 with a initial potential of − 0.2 V. Electrochemical impedance spectroscopy (EIS) was carried out in a 10 mL aqueous solution including 1.0 mM $[Fe(CN)_6]^{3-/4-}$ and 0.1 M KCl at a potential of 0.2 V over the frequency range from 0.1 Hz to 100 kHz. Differential pulse voltammetry (DPV) was executed in 10 mL PBS buffer containing HQ and H_2O_2 with the

Table 1
DNA sequences used in this assay.

Name	Sequence (5′–3′)
Tetrahedron A	ACATTCCTAAGTCTGAAACATTACAGCTTGCTACACGAGAAGAGCCGCCATAGTATTTTTTTTTTGTAGGGCAGG
Tetrahedron B	SH-C_6-TATCACCAGGCAGTTGACAGTGTAGCAAGCTGTAATAGATGCGAGGGTCCAATAC
Tetrahedron C	SH-C_6-TCAACTGCCTGGTGATAAAACGACACTACGTGGGAATCTACTATGGCGGCTCTTC
Tetrahedron D	SH-C_6-TTCAGACTTAGGAATGTGCTTCCCACGTAGTGTCGTTTGTATTGGACCCTCGCAT
Aptamer	AGTCCGTGGTAGGGCAGGTTGGGGTGACTTTTT
cDNA1	ACCCCAACCTGCCCTTT
cDNA2	ACCCCAACCTGCCCTACTTT
cDNA3	ACCCCAACCTGCCCTACCACTTT
H1	CAACCCCAGTAGTGCGGCATGGGGTT-C_6- Biotin
H2	Biotin-C_6-CACTACTGGGGTTGTGCCGAACCCCA

potential window from − 0.4V to 0.2 V, the pulse amplitude of 0.005 V, pulse width of 0.05 s and the pulse period of 0.2 s.

2.6. Gel electrophoresis

Agarose gel electrophoresis was used to characterize DNA sequences and the HCR event. the product of each step was prepared according to the experimental process. Then product solution was acted to electrophoresis analysis on the 2% agarose gel at 100 V for 60 min. After ethidium bromide staining, the gel was transferred to the GeneGenius Gel Doc system for gel imaging.

3. Result and discussion

3.1. The principle of proposed competitive aptasensor

The mechanism of the fabricated biosensor is exhibited in Scheme 1. The proposed competitive biosensor mainly composes of supporting material SN-rGO, a T-DNA probe as capture probe, target aptamers, three cDNAs, the biotin labeled harpin probe 1 (H1) and harpin probe 2 (H2). The sulphydryl T-DNA is immobilized on the AuNPs/SN-rGO/GCE which makes up an erect DNA probe due to the stereo structure of T-DNA and its upper single stranded domain designed to be complementary with cDNA partially. As described in Scheme 1(B), the base sequence of cDNA is designed to be paired with the aptamer partly, which exists rival relationship with target thrombin. Herein, in the absence of target, as shown in route b, aptamer will couple with cDNAs closely and form double helical construction, so there is no DNA strands bind with T-DNA probe and there unable to induce the following HCR. Thereby, the avidin-HRP is incapable to load on electrode and reveals little current respond. When in the presence of thrombin cDNA becomes alone because of the formation of aptamer/thrombin complexes which possesses strong competitiveness compared with cDNA. Then, the forgotten cDNA can hybridize with single stranded domain of T-DNA to unfold the loop structure of H1 and H2 to proceed the further HCR procedure. When the avidin-HRP is added, it can specific bind with biotin in H1 and H2, thus obtains a big electrochemical signal by the catalytic of HRP to the H_2O_2 + HQ system.

3.2. Characterization

As shown in Fig. 1A and B, the prepared SN-rGO was first researched by SEM and TEM. From the SEM image in Fig. 1A, ultrathin GO nanosheets can be observed, and the transparent thin film shown in of TEM image (Fig. 1B) also demonstrates the thickness of GO nanosheets is ideal. The partial folds may be attributed to the formation of deficient structures during heteroatoms-doping process of S and N (Yang et al., 2012; You et al., 2015). The SEM of AuNPs/SN-rGO/GCE is exhibited in Fig. S1A, which shows that the AuNPs are homogenous coated on rGO nanosheets. The corresponding EDS mapping analysis of C, O, N and S for SN-rGO is shown in Fig. 1C. As expected, S and N elements can be readily discerned in SN-rGO samples, suggesting that the S and N heteroatoms are infiltrated into whole rGO sheets after calefactive operation. The elementary composition of SN-rGO sample

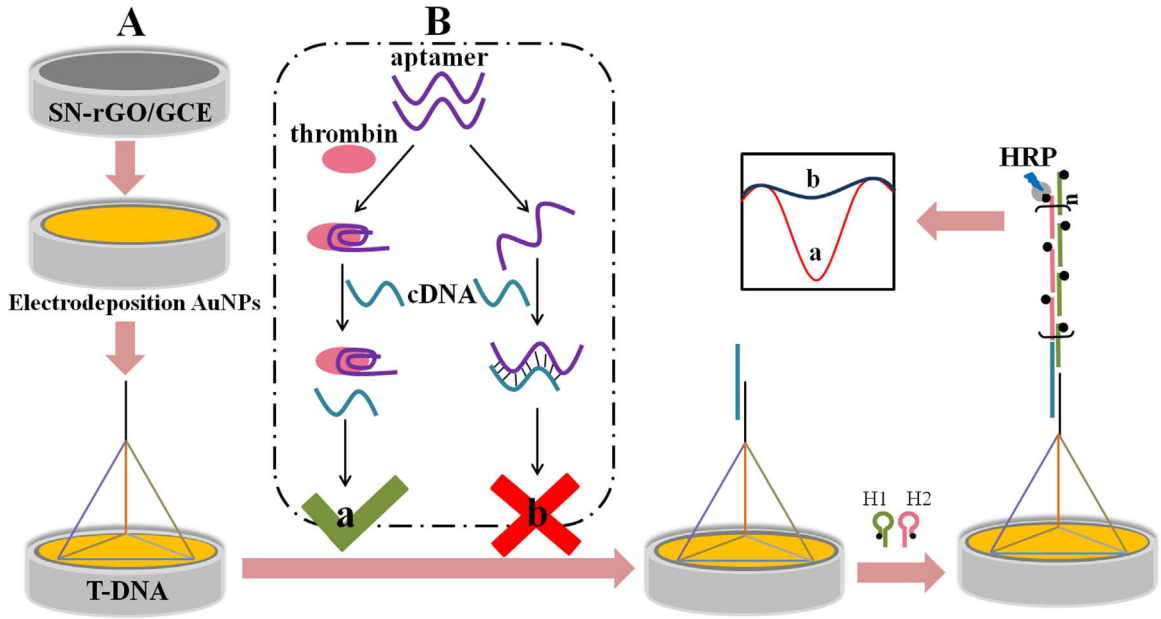

Scheme 1. Schematic diagram of the competitive aptasensor for thrombin detection.

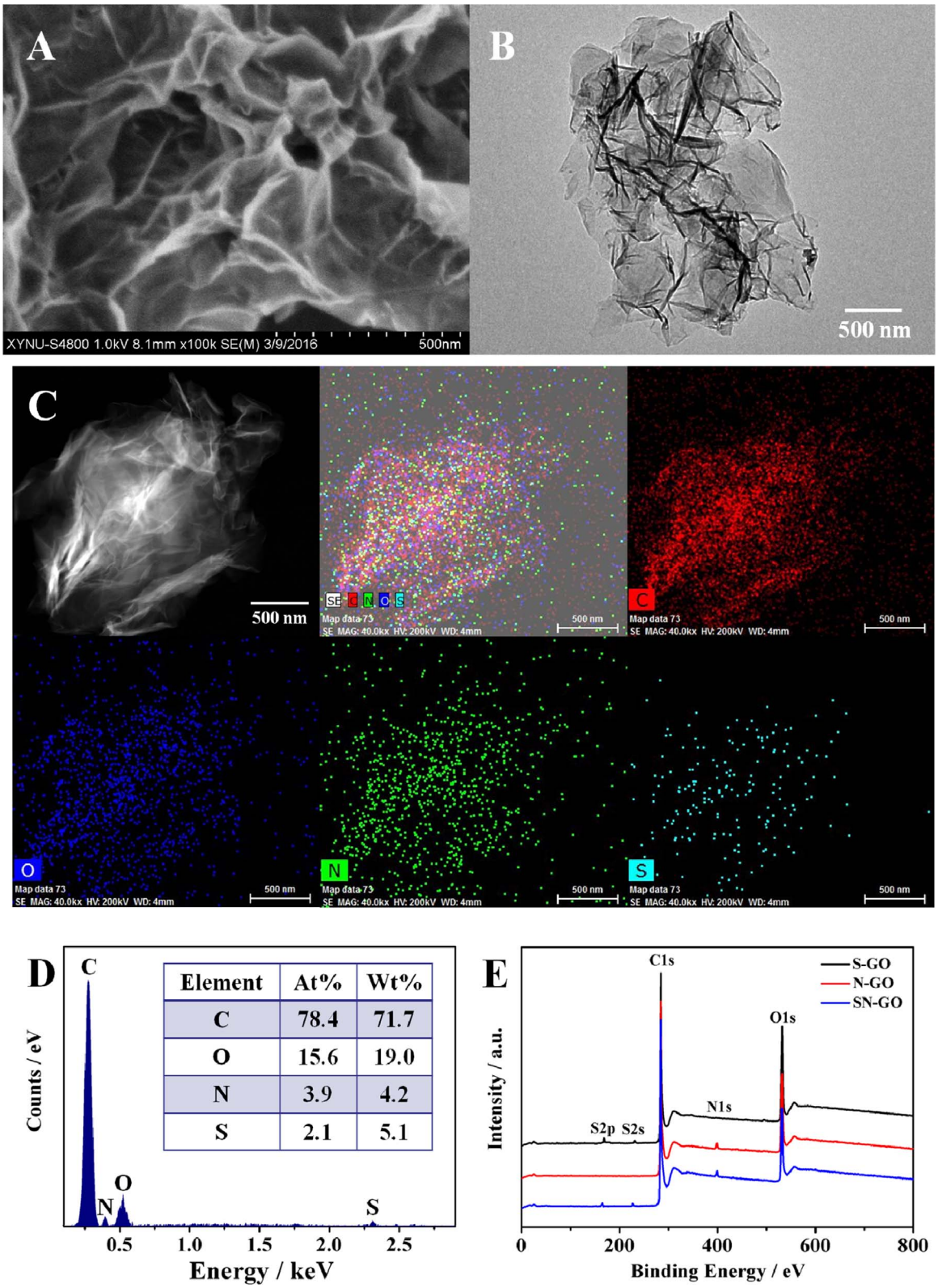

Fig. 1. SEM image (A), TEM image (B) and element mapping image (C) of prepared SN-rGO; EDS spectrum (D) of SN-rGO; XPS survey (E) of S-rGO, N-rGO and SN-rGO.

was also measured by EDS analysis (Fig. 1D). The spectrogram displays the sample is consist of C, O, N and S elements. The inset shows that the atom content and weight content of every element in the sample. The S (2.1 at%) and N (3.9 at%) element contents in the SN-rGO sample is minuscule when compared with C, indicating that the doped identity of S and N. The XPS data of S-rGO, N-rGO, SN-rGO are exhibited in Fig. 1E. Obviously, SN-rGO shows all signals of four elements in SN-rGO, demonstrating the successful doping of S and N in rGO by annealing rGO in the existence of thiocarbamide. The XPS survey offers the atom contents of C, O, S and N in SN-rGO samples for 77.7%, 16.0%, 4.1% and 2.2%, respectively, which are mainly consistent with the EDS results.

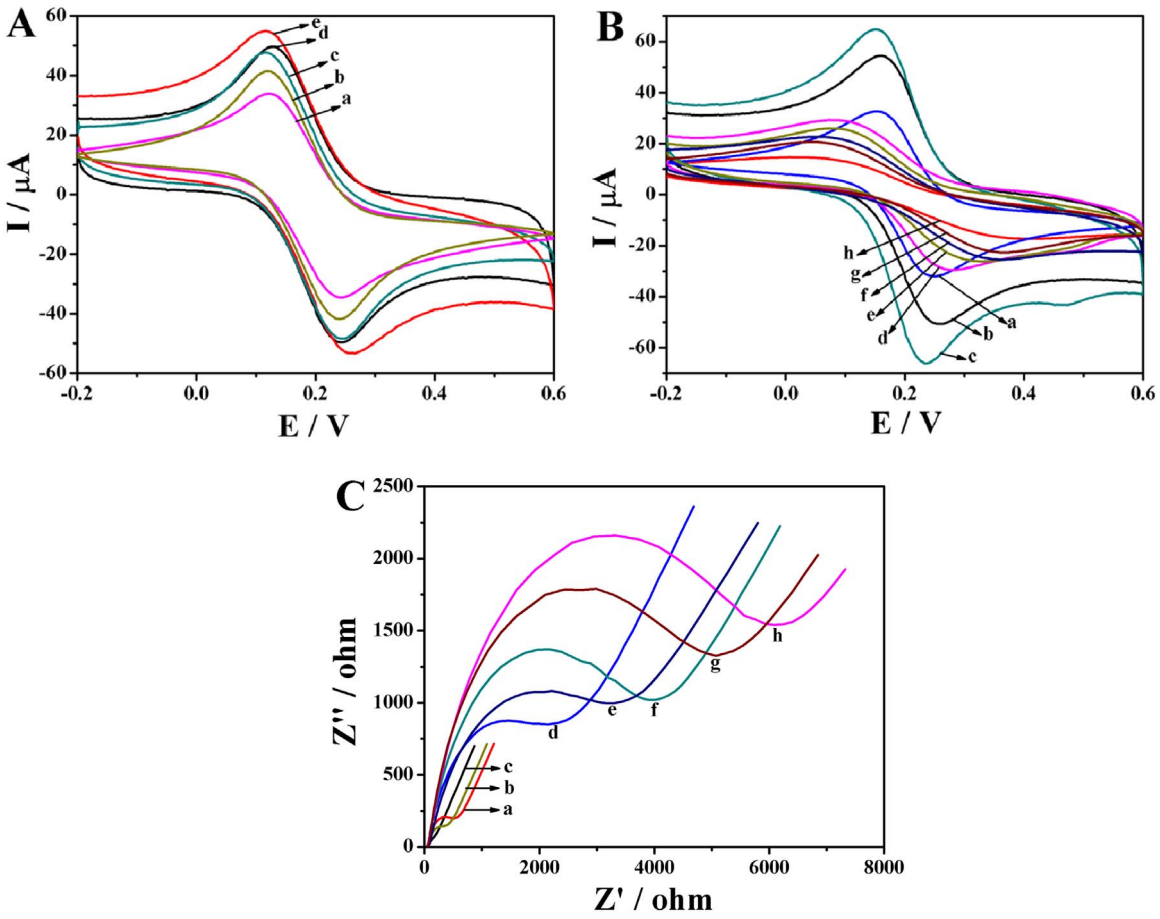

Fig. 2. CV (A) of bare GCE (a), GO/GCE (b), S-rGO/GCE (c), N-rGO/GCE (d) and SN-rGO/GEC (e); CV (B) and EIS (C) of bare GCE (a), SN-rGO/GEC (b), AuNPs/SN-rGO/GEC (c), T-DNA/AuNPs/SN-rGO/GEC (d), MCH/T-DNA/AuNPs/SN-rGO/GEC (e), cDNA/MCH/T-DNA/AuNPs/SN-rGO/GEC (f), H1-H2/cDNA/MCH/T-DNA/AuNPs/SN-rGO/GEC (g), avidin-HRP/H1-H2/cDNA/MCH/T-DNA/AuNPs/SN-rGO/GEC (h).

The SN-rGO was further characterized by using Raman spectroscopy. As can be seen in Fig. S1B, the *D* band is located at ~ 1345 cm^{-1} and is induced by the local basal plane derivatization that creates sp^3 distortion (Wang et al., 2014). The *G* band arises from the bond stretching of all sp^2-bonded pairs. The inset of Fig. S1B shows that SN-rGO generates a red-shift to 1570 cm^{-1} compared with GO sample (1580 cm^{-1}). This red-shift is an important characteristic of *n*-type substitutional doping of graphene (Yang et al., 2011; Kannan et al., 2014). The result further demonstrates the successful doping of sulfur and nitrogen atoms in the rGO.

3.3. Electrochemical characteristics

The different supporting materials were evaluated by CV. In Fig. 2A, it is obvious the redox peak currents of GO (curve b) is the lowest in four electrode materials but a little higher than bare GCE (curve a). However, The redox peak currents of SN-rGO (curve e) is higher than single-doped S-rGO (curve c) and N-rGO (curve d). This enhancement may be attributed to the valid migration of oxygen functionalities, recovery of coupling and changing of band gap (Bag et al., 2015).

The modified process step by step was also tested by CV (Fig. 2B). When SN-rGO is applied on GCE, the peak current increases (curve b) sharply compared to bare GCE (curve a), substantiating the outstanding electrochemical performance of S and N dual-doped rGO. When the AuNPs are further electrolytic deposited on SN-rGO/GEC (curve c), the current response increases immensely due to the good conductivity of AuNPs (the deposition curve of AuNPs is exhibited in Fig. S2A). Then the peak current decreases vastly (curve d) when T-DNA is immobilized on the above electrode by Au-S bond as a result of the electrostatic repulsive force between $[Fe(CN)_6]^{3/4-}$ and the negatively charged T-DNA. In like manner, the current response is further decrease (curve e) after MCH is applied on T-DNA/AuNPs/SN-rGO/GEC. This may derive from the influence of MCH which can segregate the conductive sustainer and make the electron transfer rate slow down. With the accomplish of the competitive reaction between target thrombin and cDNA, the remaining cDNA combines with the erect domain of T-DNA which aggrandizes the electrostatic repulsive force of $[Fe(CN)_6]^{3/4-}$ solution, so the electrochemical signal response reduces (curve f). After HCR procedure, current respond decreases greatly due to the formation of long DNA duplex (curve g). Finally, with the specific binding of electronegative macromolecule protein avidin-HRP, the peak current reduces again.

To further verify the events happening on the electrode surface, EIS test was carried out. Fig. 2C displays the Nyquist plots of electrode embellishment at different steps. The diameter of the semicircle in the figure can manifest the interfacial electron transfer resistance (R_{et}) of the electrode. We can see that the R_{et} value is decrease gradually from bare GCE (curve a) to SN-rGO/GEC (curve b) and AuNPs/SN-rGO/GEC (curve c), which can be attributed to the satisfactory electro-conductivity of SN-rGO and AuNPs. However, a biggish semicircle is obtained after the self-assembly of T-DNA (curve d), due to the tridimensional T-DNA as an electron transfer blocking layer hinders the charge transfer of $[Fe(CN)_6]^{3/4-}$. When MCH is used, the R_{et} observably increases (curve e). As expected, the R_{et} values all enlarge after cDNA loading (curve f) and adding plenty of H1 and H2 (curve g) to induce *in situ* hairpin polymerization. In the end, the R_{et} value increases again (curve h) when avidin-HRP is introduced in the biosensor. These EIS consequences all consistent with that of CV in Fig. 2B, demonstrating

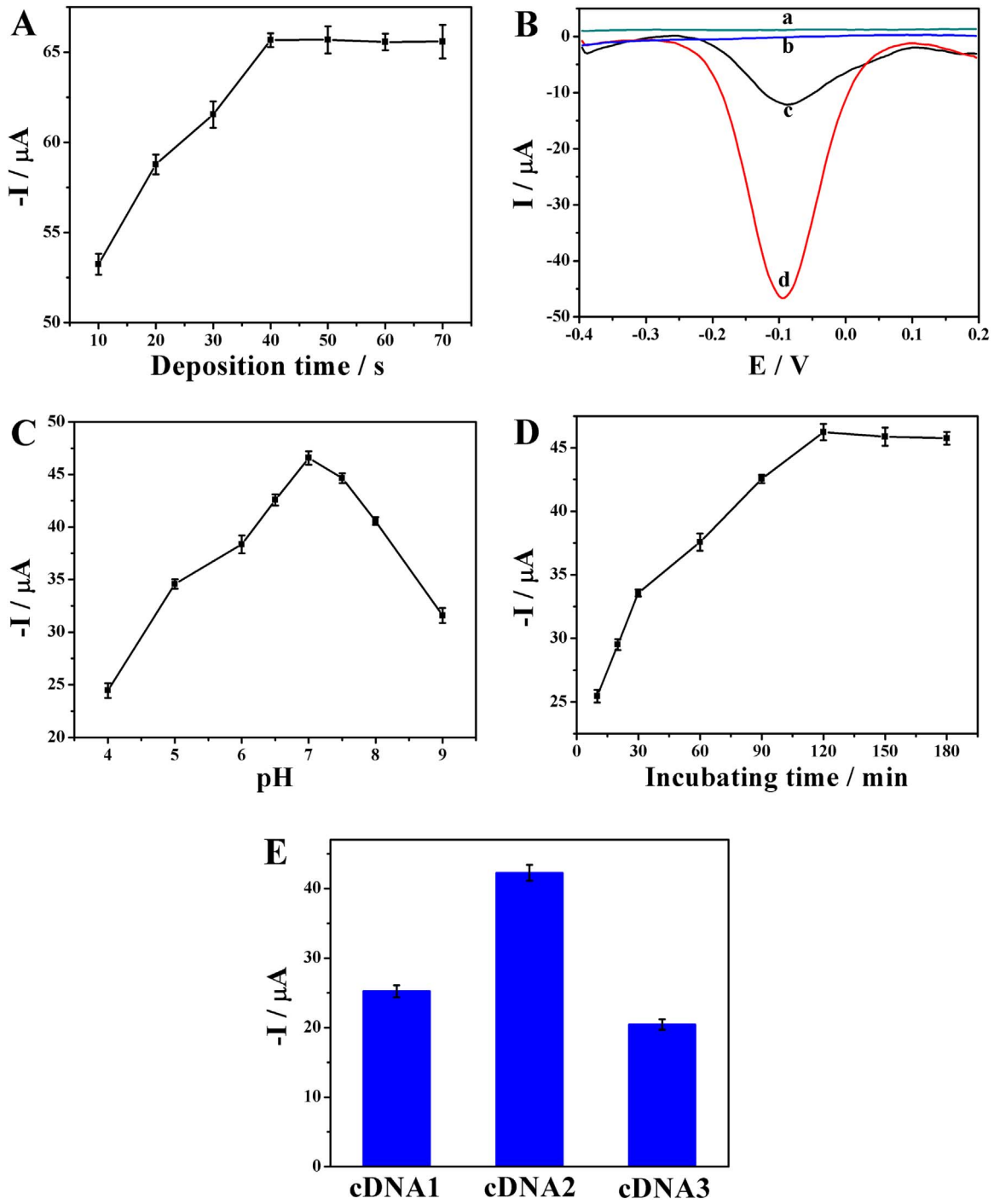

Fig. 3. (A) The current response of CV about the effect of electrodeposition AuNPs time; (B) DPVs of different electrolyte in 0.1 M PBS (pH 7.0) solution (a), containing 0.2 mM H_2O_2 (b), 0.2 mM HQ (c), 0.2 mM H_2O_2 + 0.2 mM HQ (d); (C) the effect of pH values in 0.1 M PBS containing 0.2 mM H_2O_2 + 0.2 mM HQ; (D) the effect of incubate time of H1 and H2; (E) the effect of base number of cDNA.

the successful fabrication of the competitive aptasensor.

Agarose gel electrophoresis was used to characterize DNA sequences and the HCR event. As shown in Fig. S2B, the single-stranded T-A (line 1) runs slower than T-B, C and D (line 2–4) because of the sequence of T-A is longer than the other three tetrahedron DNA chains. And the band of T-DNA (line 5) is higher than 4 ssDNAs, indicating that the tetrahedron structure of T-DNA is formed. In the absence of target (line 8), there are three independent bands of T-DNA, H1-H2 (line 6) and aptamer-cDNA (line 7) which can be ascribed that aptamer coupled with cDNA closely and formed aptamer-cDNA double-stand construction, so there is no DNA strands bind with T-DNA probe and is unable to induce the following HCR. However, in the presence of target thrombin (line 9), there are high molecular weight smeared bands on account of HCR, which also confirms that the competitive aptasensor is feasible entirely.

3.4. Optimization of experimental condition

Several experimental conditions were optimized in order to obtain the optimal experimental conditions. So the deposition time of AuNPs was tested in range of 10–70 s (Fig. 3A). The peak current increases in the deposition time range of 10–40 s because more and more AuNPs are

formed on the electrode. The current response decreases after 40 s due to the formation of the big AuNPs, which reduces the active sites. So 40 s of deposition time was used.

Fig. 3B shows the electrocatalytic activity of the avidin-HRP in different DPV electrolyte. There is no electrochemical signal when detected in PBS solution (curve a). When 2 mM HQ exists, a weak reduction peak can be observed (curve c). Nevertheless, in the sole presence of 2 mM H_2O_2 in PBS, we can't obtain electrochemical response (curve b). While a desired reduction peak appears when 2 mM H_2O_2 and 2 mM HQ concurrently exist (curve d), testifying that the avidin-HRP retains its activity and HQ acts as a valid intermediary of round-trip electrons between the electrode surface and the redox center of HRP.

The effect of electrolyte pH on DPV response was tested. As shown in Fig. 3C, a biggest peak current is obtained at pH 7.0, so pH 7.0 is selected. In this biosensor strategy, the HCR procedure plays an important role. It can immobilize more avidin-HPR to amplify electrical signal by H1 and H2, hence it's necessary to research the incubating time of H1 and H2. As displayed in Fig. 3D, 120 min is chosen as the first-rank incubating time for H1 and H2.

The impact of the sequence length of cDNA was studied. In Fig. 3E, there are three cDNAs with different length (cDNA1, cDNA2, cDNA3) are used which are complementary with aptamer partly. The cDNA1 with 17 bases shows a mezzo peak current that may due to the DNA chain is too short to fix with the vertical domain of T-DNA preferably. And then, the electrical response prominent increasing when the base number increasing to 20 (cDNA2). Whereas, further lengthening the sequence length (cDNA3 with 23 bases) cannot further increase electrical signal. This phenomenon can be explained that the longer cDNA may own stranger competitiveness than thrombin and hybridize with aptamer, impeding the hybridization between cDNA and T-DNA. Therefore, cDNA2 is chose.

3.5. Sensitivity of the biosensor

High sensitivity is an essential requirement for protein biosensor, so the sensitivity of the constructed biosensor was investigated under the optimal conditions. Fig. 4 reveals the DPV curves of thrombin ranging from 0 to 10 nM. Distinctly, the peak currents increase with increasing concentration of thrombin. The inset displays a well linear relation between the peak currents and the logarithm of the concentrations of thrombin in the range of 10^{-13}–10^{-8} M. The detection limit is 11.6 fM (S/N = 3). The linear equation is y = 7.7x – 107.28 (R^2 = 0.995), where y is the peak current and x is the logarithm of thrombin concentration. The results confirm that this competitive signal-amplification biosensor is competent to the sensitive measurement of target protein thrombin, and it reveals a better and comparable property contrasts with the antecedent reportorial references (Table S1).

3.6. Selectivity, reproducibility and stability

We have contrasted the DPV responses in the cases of five different proteins (1.0 nM) including CEA, PDGF-BB, BSA, thrombin and the mixture of these four kinds of proteins (Fig. 4B). The data manifests that only thrombin and the mixture which contains thrombin can acquire prominent increases of peak currents than blank. The peak currents of other three proteins show little difference with the blank. This good selectivity of the biosensor can be ascribed to the high specificity and affinity between the aptamer and target thrombin. Furthermore, six uniform electrodes were used to monitor 0.1 nM thrombin by DPV and gained relative standard deviation (RSD) of 3.9%, indicating its good reproducibility. Moreover, the stability of biosensor was studied by reserving under 4 °C for 20 days. 91.3% of the original peak current to 0.1 nM thrombin can still be left, indicating its good stability.

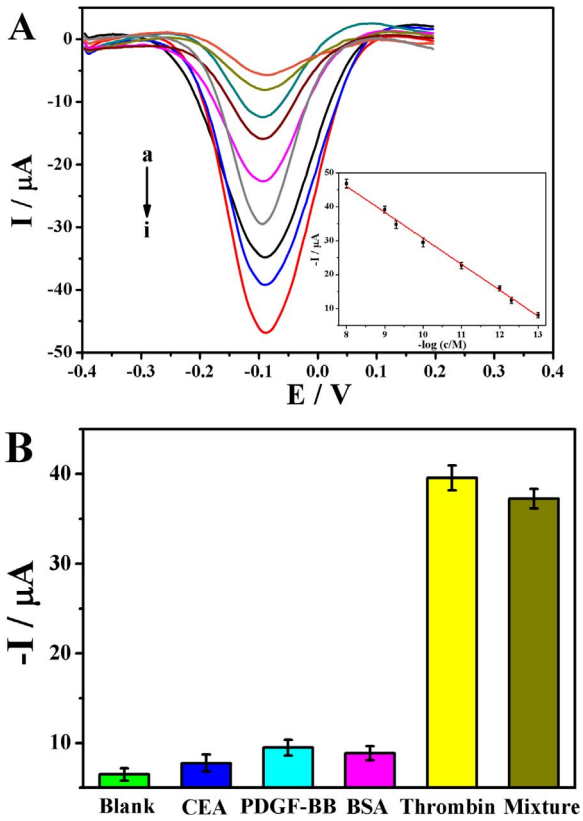

Fig. 4. (A) DPV of different concentrations of thrombin (a–i): 0 , 1×10^{-13}, 5×10^{-13}, 1×10^{-12}, 1×10^{-11}, 1×10^{-10}, 5×10^{-10}, 1×10^{-9}, 1×10^{-8} M. Inset shows the DPV peak current value versus the logarithmic concentration of thrombin. (B) The DPV of blank, 1.0 nM CEA, 1.0 nM PDGF-BB, 1.0 nM BSA, 1.0 nM thrombin and the mixture of four kinds of these proteins with 1.0 nM.

3.7. Real samples detection

For the sake of evaluating the feasibility of the developed competitive sensor for thrombin detection, the practical flexibility was researched. Different concentrations of thrombin were added into healthy human real serum samples acquired from the Xinyang Central Hospital, (Xinyang, China). Each sample was detected for three times and the detection value took the average. As is shown in Table S2, recoveries are in the range of 94.5–103.1%, and RSDs are ranging from 3.3 to 5.7, suggesting that the present biosensor is available for monitoring thrombin in real samples.

4. Conclusion

A competitive signal-amplification aptasensor is fabricated for sensitive detection of thrombin and shows outstanding advantages. Firstly, the conductivity and specific surface area of electrode are enhanced with the usage of SN-rGO as the electrode substrate, which is preferable for accelerating electron transfer and loading more DNA probe, therefore lower the detection limit. Secondly, the T-DNA probe can control the density and orientation as well as surmount the spatial effect compared with a conventional single-stranded probe at the electrode interface. Thirdly, the firm binding force of aptamer-target thrombin conjugates competes with cDNA which spark subsequent HCR and thus produces a strong current respond to further decrease the detection limit. The last but not least, in the detection system, HQ recycles and H_2O_2 assists in accomplishing it and results in augment of the electrochemical response acts on avidin-HRP. Based on these preponderances, the constructed biosensor can detect target thrombin down to 11.6 fM with good selectivity.

Acknowledgments

This work was supported by the National Natural Science Foundation of China (21475115), Program for University Innovative Research Team of Henan (15IRTSTHN001), Henan Provincial Science and Technology Innovation Team (C20150026), Nanhu Scholars Program of XYNU, Henan Science and Technology Cooperation Project (172106000064) and Graduate Scientific Research Innovation Fund of Xinyang Normal University (No. 2016KYJJ12).

Appendix A. Supporting information

Supplementary data associated with this article can be found in the online version at http://dx.doi.org/10.1016/j.bios.2017.09.022.

References

Bag, S., Mondal, B., Das, A.K., Raj, C.R., 2015. Electrochim. Acta 163, 16–23.
Bichler, J., Heit, J.A., Owen, W.G., 1996. Thromb. Res. 84, 289–294.
Cardoso, A., Cabral-Miranda, G., Reyes-Sandoval, A., Bachmann, M.F., Sales, G.F., 2017. Biosens. Bioelectron. 91, 833–841.
Chen, X.J., Pan, Y.J., Liu, H.Q., Bai, X.J., Wang, N., Zhang, B.L., 2016a. Biosens. Bioelectron. 79, 353–358.
Chen, L., Song, L.P., Zhang, Y.C., Wang, P., Xiao, Z.D., Guo, Y.G., Cao, F.F., 2016b. ACS Appl. Mater. Interfaces 8, 11255–11261.
Dirks, R.M., Pierce, N.A., 2004. Proc. Natl. Acad. Sci. USA 101, 15275–15278.
Du, R.J., Zhu, L.N., Gan, J.R., Wang, Y.N., Qiao, L., Liu, B.H., 2016. Anal. Chem. 88, 6767–6772.
Duan, X.G., O'Donnell, K., Sun, H.Q., Wang, Y.X., Wang, S.B., 2015. Small 11, 3036–3044.
Ellington, A.D., Szostak, J.W., 1990. Nature 346, 818–822.
Ha, N.R., Jung, I.P., La, I.J., Jung, H.S., Yoon, M.Y., 2017. Sci. Rep. 7, 40305–40314.
Hou, Y.N., Liu, J.F., Hong, M., Li, X., Ma, Y.H., Yue, Q.L., Li, C.Z., 2017. Biosens. Bioelectron. 92, 259–265.
Huang, K.J., Liu, Y.J., Wang, H.B., Wang, Y.Y., 2014. Electrochim. Acta 118, 130–137.
Huang, K.J., Liu, Y.J., Zhai, Q.F., 2015. J. Mater. Chem. B 3, 8180–8187.
Huang, K.J., Shuai, H.L., Zhang, J.Z., 2016. Biosens. Bioelectron. 77, 69–75.
Hummers, W.S., Offeman, R.E., 1958. J. Am. Chem. Soc. 80 (1339-1339).
Jeddi, I., Saiz, L., 2017. Sci. Rep. 7, 1178.
Kannan, A.G., Zhao, J., Jo, S.G., Kang, Y.S., Kim, D.W., 2014. J. Mater. Chem. A 2, 12232–12239.
Kuang, L., Cao, S.P., Zhang, Li, Li, Q.H., Liu, Z.C., Liang, R.P., Qiu, J.D., 2016. Biosens. Bioelectron. 85, 798–806.
Li, N.X., Chen, J.Y., Luo, M., Chen, C.H., Ji, X.H., He, Z.K., 2017. Biosens. Bioelectron. 87, 325–331.
Li, Y., Xu, J., Wang, L., Huang, Y., Guo, J., Cao, X., Shen, F., Luo, Y., Sun, C., 2016. Sens. Actuators B – Chem. 222, 815–822.
Lin, M.H., Song, P., Zhou, G.B., Zuo, X.L., Aldalbahi, A., Lou, X.D., Shi, J.Y., Fan, C.H., 2016. Nat. Protoc. 11, 1244–1263.
Liu, H.Y., Bei, X.Q., Xia, Q.T., Fu, Y., Zhang, S., Liu, M.C., Fan, K., Zhang, M.Z., Yang, Y., 2016. Microchim. Acta 183, 297–304.
Lv, S.Z., Zhang, K.Y., Lin, Z.Z., Tang, D.P., 2017. Biosens. Bioelectron. 96, 317–323.
Miao, P., Tang, Y.G., Yin, J., 2015. Chem. Commun. 51, 15629–15632.
Nguyen, V.T., Kwon, Y.S., Gu, M.B., 2017. Curr. Opin. Biotechnol. 45, 15–23.
Pelzer, H., Schwarz, A., Heimburger, N., 1988. Thromb. Haemost. 59, 101–106.
Poturnayová, A., Šnejdárková, M., Castillo, G., Rybár, P., Leitner, M., Ebner, A., Hianik, T., 2015. Chem. Pap. 69, 211–226.
Singh, S., Tuteja, S.K., Sillu, D., Deep, A., Suri, C.R., 2016. Microchim. Acta 183, 1729–1738.
Shuai, H.L., Huang, K.J., Huang, Xing, L.L., Chen, Y.X., 2016. Biosens. Bioelectron. 86, 337–345.
Shuai, H.L., Huang, K.J., Huang, Wu, X., 2017. J. Mater. Chem. B 5, 5362–5372.
Shuman, M.A., Majerus, P.W., 1976. J. Clin. Investig. 58, 1249–1258.
Taghdisi, S.M., Danesh, N.M., Ramezani, M., Abnous, K., 2016. Biosens. Bioelectron. 85, 509–514.
Tan, L.L., Chen, Z.B., Zhang, C., Wei, X.C., Lou, T.H., Zhao, Y., 2017. Small 13 (14), 1603370.
Wang, Y.,H., Huang, K.J., Wu, X., 2017. Biosens. Bioelectron. 97, 305–316.
Wang, X., Wang, J., Wang, D., Dou, S., Ma, Z., Wu, J., Tao, L., Shen, A., Ouyang, C., Liu, Q., Wang, S., 2014. Chem. Commun. 50, 4839–4842.
Yang, Z., Yao, Z., Li, G., Fang, G., Nie, H., Liu, Z., Zhou, X., Chen, X., Huang, S., 2011. ACS Nano 6, 205–211.
Yang, S.B., Zhi, L.J., Tang, K., Feng, X.L., Maier, J., Mullen, K., 2012. Adv. Funct. Mater. 22, 3634–3640.
Yang, Y., Yang, Z.H., Lv, J.J., Yuan, R., Chai, Y.Q., 2017. Talanta 169, 44–49.
Ye, J.Q., Zhang, Y., Huang, H., Wang, J., Jiang, Z., Bai, M., 2017. Sens. Actuators B – Chem. 243, 1255–1260.
You, J.M., Ahmed, M.S., Han, H.S., Choe, J.E., Üstündag, Z., Jeon, S., 2015. J. Power Sources 275, 73–79.
Zhao, M., Liao, N., Zhuo, Y., Chai, Y.Q., Wang, J.P., Yuan, R., 2015. Anal. Chem. 87, 7602–7609.
Zhao, X.P., Cao, J., Nie, X.G., Wang, S.S., Wang, C., Xia, X.H., 2017. Electrochem. Commun. 81, 5–9.